Geomechanics and Engineering, *Vol. 43, No. 4 (2025) 315-327*
https://doi.org/10.12989/gae.2025.43.4.315

Response of soft clay improved with electrokinetic-assisted encased stone column

B.K. Pandey*[1] and S. Rajesh[2a]

[1]*Department of Civil Engineering, Guru Ghasidas Vishwavidyalaya, Koni, Bilaspur 495009, Chhattisgarh, India*
[2]*Department of Civil Engineering, Indian Institute of Technology Kanpur, Kanpur 208016, Uttar Pradesh, India*

(*Received October 6, 2024, Revised September 21, 2025, Accepted November 7, 2025*)

Abstract. The improvement of marginal sites requires both technically appropriate and sustainable ground modification techniques to mitigate the geotechnical issues associated with the site encountered. This study evaluated the response of soft clay improved with an electrokinetic-assisted encased stone column. In this study, the stone columns were encased with conductive natural geotextile to incorporate electrokinetic coupling, enhancing the clayey soil performance. The prepared electrokinetic-assisted encased stone column acts as a cathode during the coupling process, and mild steel bars were used as an anode material. The electrokinetic process was initiated by applying a voltage gradient across electrodes (i.e., anode and cathode). The research highlights the impact of combining electrokinetics with an encased stone column (ESC) on the strength, deformation, and physicochemical and structural response of clayey soil. During the experiment, the discharge of pore water, vertical deformation, and current were continuously monitored to evaluate the method's effectiveness. At the culmination of the test, the reduction in soil moisture, improvement in undrained shear strength, anode deterioration, and changes in the soil's physicochemical, mineralogical, and structural properties were assessed. The results indicate that coupling electrokinetics with an ESC significantly accelerates pore water removal efficiency, and approximately 14% higher settlement was observed for the 0.15 V/mm compared to the ESC case. The time to remove 95% of the total pore water was reduced by approximately 87% with a voltage gradient of 0.15 V/mm compared to the ESC. The undrained shear strength increases with an increase in applied voltage gradient and with depth. As compared to the ESC case, the undrained shear strength increases by 1.23, 1.43, 1.58, and 1.80 times for applied voltage gradients of 0.025, 0.05, 0.10, and 0.15 V/mm. This study also shows significant changes in moisture content, physicochemical properties, mineralogy, and soil structure.

Keywords: clay; electrokinetics; encased stone column; natural geotextile; strength; voltage gradient

1. Introduction

Large number of infrastructures are required to accommodate tremendous population growth. The Sustainable Development Goals (SDGs) outlined by the United Nations (UN) must be incorporated into infrastructure projects to achieve economically, socially, and environmentally sustainable development. With land scarcity, infrastructure projects may have to be built on unsuitable sites, which poses severe design and operational challenges (Hunter *et al.* 2021). Infrastructure built on problematic soil can cause significant financial and human consequences due to stability issues. Problematic soil may possess diverse characteristics like excessive settlement, collapse potential, low undrained shear strength, and expansive and corrosive behavior (Hausmann 1991). Problematic soil characteristics can limit design options, causing developers to abandon projects. To meet design requirements, one solution is to alter the soil through ground improvement techniques (Hausmann 1991, Malarvizhi and Ilamparuthi 2007). There are numerous ground improvement techniques like mechanical stabilization, preloading, grouting, chemical stabilization, dewatering, granular columnar inclusions, stone columns, soil reinforcement, replacing the soil with suitable sustainable materials, use of geosynthetic materials and coffee husk, etc. (Hausmann 1991, Rajesh 2017, Dinarvand and Ardakani 2022, Pandey *et al.* 2022a, Jaiswal and Kumar 2023, Al-Khafaji *et al.* 2024, Sun *et al.* 2024) for improving the geotechnical issues of problematic soils. Among these improvement methods, the application of an encased stone column (ESC) for improving the clayey soil having low (<15 kPa) strength (Pandey *et al.* 2022a) is acknowledged. The column's encasement helps constrain the bulging by providing lateral confinement (Demir and Sarici 2017, Rajesh 2017, Pandey *et al.* 2022b, Zhang *et al.* 2022) to the column materials.

In the last two decades, numerous research has been conducted (Rajesh 2017, Pandey *et al.* 2021, Zhang *et al.* 2022) to recognize the implications of characteristic properties of ESC and clayey soil in improving strength, deformation and hydraulic performance of clayey soil enhanced by the inclusion of ESC. Further, the most predominant material used to construct columns is concrete debris, natural gravel, crushed limestone, and brick rubble

*Corresponding author, Assistant Professor
E-mail: balbirpandey123@gmail.com
[a]Professor
E-mail: hsrajesh@iitk.ac.in

ISSN: 2005-307X (Print), 2092-6219 (Online)

(Yu *et al.* 2020, Pandey *et al.* 2022a). However, considering the proper disposal of various industrial waste and their practical utilization, waste materials like waste tires (Mazumder *et al.* 2018), steel slag (Rezaei-Hosseinabadi *et al.* 2022), and fly ash (Dutta and Mandal 2017) have also been utilized for the construction of stone column. The encasement of the stone columns in previous studies and field implementations is predominantly constructed of geosynthetic materials (Rajesh 2017, Pandey *et al.* 2022a, 2022b). The geosynthetic materials used are geotextiles (both woven and non-woven) (Murugesan and Rajagopal 2007; Tandel *et al.* 2014) and geogrids (Malarvizhi and Ilamparuthi 2007), other synthetic materials (Zhang *et al.* 2012). The studies have also considered the effect of encasement parameters (like their stiffness and length) (Pandey *et al.* 2022b). The existing literature emphasizes that limited studies have been conducted on using natural geotextiles as encasement material. If utilized as an encasement, natural geotextiles could eventually blend in with the clayey soil because they degrade naturally, have no adverse environmental effects (Methacanon *et al.* 2010), and can be a sustainable alternative. Despite having a shorter lifespan, natural jute geotextiles have advantages if used as an encasement for a stone column in confinement to column material and accelerating the consolidation settlement.

However, in certain situations where the permeability of the clayey soil is extremely low, and if there is a compulsion to accelerate the consolidation process, coupling the electrokinetics with other ground improvement methods can be effectively utilized. The electrokinetic treatment is a sustainable soil remediation and improvement technique that involves inducing the movement of charged particles in soil by applying a low-voltage electric field between electrodes embedded in the ground. This field causes cations and anions in the soil's diffuse double layer (DDL) to migrate toward the cathode and anode, respectively. As a result, various physico-chemical transport processes are triggered, facilitating the extraction of pore water, as well as organic, inorganic, and heavy metal contaminants from the soil (Jones *et al.* 2011, Zhou *et al.* 2015, Pedersen *et al.* 2018, Pandey and Rajesh 2019, Hamza and Ikin 2020). Mohamedelhassan and Shang (2001) and later Bergado *et al.* (2003) attempted to understand the impact of electrode material and current intermittence after electrokinetics is coupled with surcharge loading. Further, to enhance the efficiency of the coupled phenomena, a saline solution was injected at the anode (Chien *et al.* 2009). Similarly, if the encased stone column is coupled with electrokinetics, as first attempted by Pandey *et al.* (2021), it will have benefits like increasing the dewatering efficacy and altering the physicochemical properties and structure of the clayey soil. Apart from the mentioned study, a few other studies have reported coupling electrokinetics with vertical drains and vacuum preloading (Wang *et al.* 2020, Zhuang 2021). The existing literature underlines that limited attempts have been made to understand the deformation, strength, physicochemical, and structural response of clayey soil improved with electrokinetics-assisted ESC.

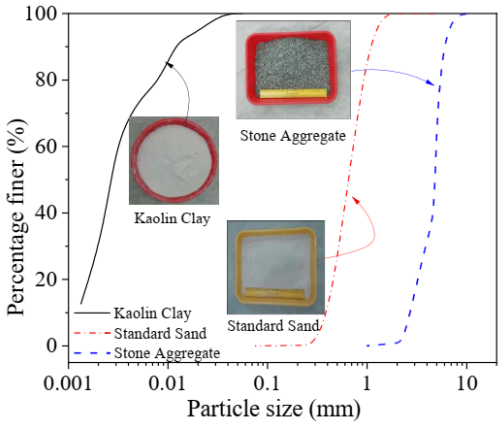

Fig. 1 Particle size distribution of kaolin clay, standard sand, and stone aggregate

This study was conducted to establish the impact of the electrokinetics-assisted ESC on the strength, deformation, physicochemical, and structural response of clayey soil. There are two goals for this investigation. The first is to construct the encasement of the stone column using conductive geotextile. The second is to evaluate the effectiveness of electrokinetics-assisted ESC on the discharge of pore water and vertical deformation, lessening the moisture content, and enhancing the strength of the clayey soil. Further, it also sheds light on operational variables like current variation, power consumption, and deterioration of anode material. Ultimately, it assesses the impact of electrokinetic coupling on the physicochemical, mineralogical, and structural modification of the clayey soil. Subsequently, a trend line was included to fit the experimental data.

2. Materials, methods, and processes

2.1 Material characteristics

The powder kaolin was used to create the clay bed. The drainage layer was made from the standard sand (Grade II), and the stone column was constructed from stone aggregate procured locally. Fig. 1 depicts standard sand (grade II), kaolin clay, and stone aggregate particle size distribution. The standard sand depicted in Fig. 1 is Indian Standard sand (commercially known as Ennore sand) of Grade II (IS 650: 2008) procured from Tamil Nādu Minerals Limited, India. As noticed in Fig. 1, 100% of kaolin particles are finer than 0.075 mm. Further, approximately 30% of the particles are finer than 0.002 mm. The particle sizes of the stone aggregates ranged from 1 to 6.5 mm. However, 100% of particles of standard sand were less than 2 mm. Tables 1 and 2 provide the essential geotechnical characteristics of kaolin clay, standard sand, and stone aggregate. According to the USCS soil classification system, the powdered kaolin utilized in the study is categorized as inorganic clay of high plasticity (CH). At the same time, stone aggregate and standard sand were identified as poorly graded gravel (GP) and poorly graded sand (SP).

Table 1 The basic geotechnical properties of kaolin clay

Property	Value
Natural water content (%)	0.76
The specific gravity of soil solids (G)	2.64
Gradation (%)	
Sand	0
Silt	70.25
Clay	29.75
Atterberg limits	
Liquid limit, w_L (%)	51
Plastic limit, $w_{P\,(\%)}$	27
Permeability (x10^{-9} m/s)	5.09
Compressibility index (C_c)	0.14
Moisture density relationship	
Optimum moisture content (%)	24.6
Maximum dry unit weight (kN/m^3)	15.20
pH	8.53
SSA (m^2/g)	17.88
CEC (meq/100 g)	1.94
Swelling Potential Classification	Low
Zeta potential (mV)	-21.84

Table 2 The basic geotechnical properties of stone aggregate and standard sand

Properties	Magnitude	
	Stone aggregate	Standard sand
Coefficient of uniformity, C_u	1.83	1.90
Coefficient of curvature, C_c	1.12	0.97
USCS classification	GP	SP
Cohesion intercept (kPa)	0	0
Angle of internal friction $\emptyset^\circ$	49.37	34.09
Coefficient of permeability (m/s)	3.72 x 10^{-5}	1.96 x 10^{-5}
Poisson's ratio υ	0.33	0.33
Constrained modulus (kPa)	38844.96	10000

A local vendor supplied the natural jute geotextile to construct a conductive geotextile encasement. Table 3 displays the characteristics of the jute geotextile obtained following the relevant standards as listed in it. Because jute has a lower tensile strength than synthetic geotextiles, the test was conducted at a constant rate of strain of 40 mm per minute due to the low strength of the materials, although ASTM D4595-17 proposes a strain rate of 10 ± 3 %/min for conducting a wide-width tensile strength test. However, the geotextile used in the present case was a natural jute geotextile; the textile strands fail quickly at such a fast strain rate.

2.2 Test apparatus and sample preparation procedure

With an interior diameter and height of 256 and 500 mm, respectively, the clay bed for the model test was constructed in a specially developed test setup. The test setup diameter was designed to have the least possible

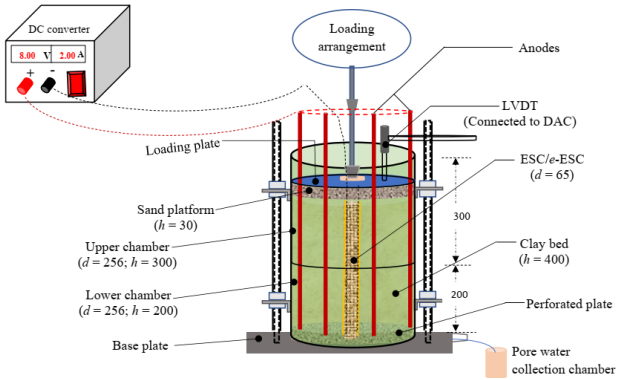

Fig. 2 The schematic of the test setup, along with their details (All dimensions are in mm)

impact of the boundary on the test result (Chummar 1972) for the chosen 65 mm diameter of ESC. The setup height consists of two separable cylindrical cells, the top and bottom cell heights are respectively 300 and 200 mm. The top half had vertical splits, firmly fastening two half rounds, ensuring no joint leaks. The split was made available to make sampling easier after the test. Fig. 2 shows the test setup's schematic and constituent parts in their simplest form. Further, internally attached grooves were carved in the base plate. The grooves were connected to the collecting chamber through a specially designed vent in the base plate. The discharge water was collected in the collection chamber and was measured to determine its variation.

The encasement was made utilizing conductive natural geotextile, and preceding discussions on the essential characteristics of the geotextile were used to prepare it. The geotextile was trimmed and formed into a cylinder to create the encasement. A 20 mm overlap of the geotextile, properly stitched, formed the longitudinal joint required to build the sleeve, as shown in Fig. 3(a). The tensile strength test was performed with a different trial stitched pattern, and the stitching pattern giving tensile strength close to the original specimen was chosen to prepare the longitudinal joint of the encasement. The geotextile fabric is created with material ribs intersected during manufacture, one along the machine direction (MD) and the other across it, known as cross-machine direction (CMD). A 0.57 mm copper wire was intertwined into the natural geotextile at a circumferential arrangement with a spacing of 29 mm in the cross-machine direction to make it conductive (refer to Figs. 3(b) and 3(c)). This natural geotextile intertwined with copper wire is named as conductive natural geotextile in this study. The presence of copper wire threads is expected to have minimal impact on the strength in the machine direction. In the experiment, a voltage gradient was employed to start the electrokinetics process, and the conductive natural geotextile encasement served as the cathode.

The specifics and test conditions for the experiments carried out for this investigation are presented in Table 4. The clayey soil improved with an encased stone column without voltage gradient is referred to as the ESC case, whereas ESC coupled with electrokinetics is designated an e-ESC case. The experiments were carried out on the foundation bed having an

Fig. 3 Various components of the test procedure (a) adopted pattern for making encasement, (b) prepared encasement with a marking for inclusion of copper wire, (c) prepared encasement, (d) sample kept for moisture equilibrium, (e) confirming the strength of prepared clay bed, (f) preparation of column, (g) prepared clay bed improved with ESC/e-ES, (h) prepared drainage layer and (i) prepared final sample

undrained shear strength (Su) of 10 kPa, measured using a pocket vane shear tester. To achieve the required strength, the powder kaolin was mixed thoroughly with an adequate amount of ultrapure (Milli-Q) water, ensuring no lumps were left to attain the desired moisture content of 35%. The desired moisture content corresponded to approximately 10 kPa undrained shear strength and was fixed based on various trials of strength variation with moisture content. The thoroughly mixed wet clay is kept for 24 hours in airtight polythene bags to maintain moisture equilibrium, as shown in Fig. 3(d).

A perforated plate was placed at the bottom of the tank before sample preparation started followed by the placement of a circular geotextile over it. The pipe with an encasement was positioned in the middle of the mold before the clay foundation bed was constructed. The needed undrained shear strength 400 mm thick clay bed was built in layers, each 50 mm thick (Pandey *et al.* 2021). Every layer was spread evenly, and any trapped air within them was removed by hand compaction. The undrained shear strength of each compacted layer is evaluated using a pocket vane tester as depicted in Fig. 3(e), and moisture content at the time of placement was also checked for uniformity in sample clay bed preparation.

The column construction (SC/ESC/e-ESC) is started once the soft soil bed attains the target height (i.e., 400 mm). The

Table 3 The properties of the jute geotextile

Properties		Value	Relevant Standard
Thickness under 2 kPa (mm)		0.96	ASTM D5199-12
Mass per unit area (g/m^2)		357.8	ASTM D5261-10
Width (m)		0.89	IS:1954.2002
Permittivity (s^{-1})		0.19	ASTM D4491M-17
Tensile strength (Wide-width method), (kN/m)	MD*	24.33	ASTM D4595-17
	CMD**	5.17	
Strain at Peak strength (%)	MD	4.82	ASTM D4595-17
	CMD	3.88	
Secant stiffness at failure strain (kN/m)	MD	504.50	BS EN ISO 10319 (2015)
	CMD	136.57	

eight layers of stone aggregate were placed into the cylindrical pipe, having a determined quantity for each layer with a goal height of 50 mm. to attain the prescribed relative density of 76%. Each layer of placed column material was compacted using a tamping rod having an enlarged base equal to 60 mm and compacted ten times. The pipe was then withdrawn in phases (refer to Fig. 3(f)), ensuring each phase removal of 30 mm. This was the strategy for constructing the column; however, for ESC/e-ESC, the encasement was warped outside the surface of the pipe, and the remaining steps remained the same. The encasement of the stone column was full (throughout the length). Further, the constructed ESC/e-ESC was firmly on the perforated base of the chamber. The completed height of the clay bed improved with ESC/e-ESC as shown in Fig. 3(g). After clay bed preparation with ESC/e-ESC is complete, to prevent the sand and clay bed from combining, a filter paper was placed on top of it. A filter paper was placed on top to avoid intermixing sand and clay beds. A predetermined quantity of standard sand was chosen for constructing the drainage layer. The thickness of the drainage layer constructed in the process is 30 mm. Fig. 3(h) demonstrates the completed drainage layer, the top permeable layer.

The entire test setup area, including a clay bed with ESC/e-ESC, is subjected to vertical loading. The loading resulted in equal strain in both the column and the clay. The force is transferred uniformly and applied via a lever arm mechanism; however, the distribution of stresses was not monitored. The plunger is attached to the lever arm lying on a thin steel plate, as shown in Fig. 2. A high-density polypropylene loading plate supports the smaller plate with a 253 mm diameter and 15.5 mm thickness. The loading plate was provided with holes of a diameter of 9.5 mm for the placement of anodes. The openings were made at a circumferential distance of 105 mm, more than 12 times the diameter of the anodes. The anode rods adopted in this research were mild steel bars of 8 mm in diameter and 600 mm long. The placed anodes through the hole of the loading plate do not interfere with the settlement of the plate due to the 1 mm clearance provided in the hole. A total of seven anode rods were used in the experiment, as shown in Fig. 3(i). At this

Table 4 Experimental details and test conditions

Foundation System	Undrained Shear strength** (kPa)	Voltage Gradient (E) (V/mm)	Anode
ESC	9.70	0	NA
e-ESC	10.25	0.025	Mild steel
	9.91	0.05	Mild steel
	10.14	0.10	Mild steel
	10.47	0.15	Mild steel

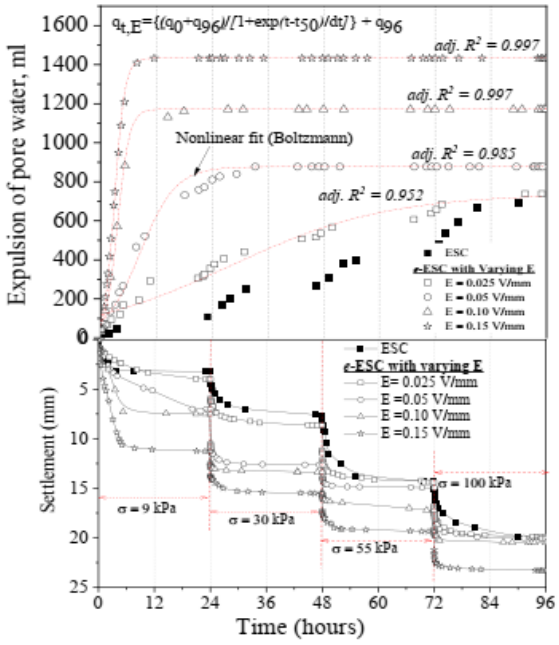

Fig. 4 Influence of applied voltage gradient on the discharge of pore water and settlement

stage, the sample prepared in the setup is complete in all respects and ready for testing to begin. As mentioned earlier, the encasement of the stone column comprises conductive jute geotextile, which acts as a cathode during electrokinetic coupling. Four steps of the vertical load were applied to the unit cell to represent the embankment construction procedure. The applied stage load produced cumulative stress of 9, 30, 55, and 100 kPa, and each load was sustained for 24 hours. Therefore, the total time taken from the start of the sample preparation to the completion of the test is about 132 hours, of which 96 hours is the actual testing time.

A linear variable differential transformer (LVDT) of sensitivity 0.01 mm measured the surface settlement. A regulated dual DC power supply was applied to the DC power supply (model LD3205). The power supply works at an input voltage of 230V AC plus or minus 10%, 50 Hz, 1 phase, with a regulated output voltage of 0-32 V, having a current varying in the range 0-5 A determined by impedance load.

In conclusion, a pocket vane tester assessed undrained shear strength at the top and mid-depth of the soft clay layer at radial distances (r) of 48, 78, and 108 mm from the column's center. After determining the undrained shear strength at each location, soft clay samples were collected to determine water content after the culmination of the test (i.e., 100 kPa load). Following Pandey *et al.* (2021), the alteration in the physicochemical and structural parameters of the clay was assessed using samples taken from the mid-depth.

3. Experimental results and discussion

3.1 Discharge of pore water and settlement

Fig. 4 shows how the voltage gradient affects the pore water discharge over time. The overall amount of pore water discharged increased as the voltage gradient rose. For applied voltage gradients of 0.15, 0.1, 0.05, and 0.025 V/mm, e-ESC improved clay; the discharge was 2.01, 1.65, 1.23, and 1.04 times the discharge in the case of ESC, respectively. The discharge variation follows a non-linear Boltzmann curve and is given by Eq. (1). The final discharge of 0.025 v/mm is insignificant (i.e., approximately 3.5% higher) compared to the ESC case. The time taken for removing 50% of the total discharge is reduced by approximately 46 % compared to the ESC case. Regression analysis in Eq. (2) reveals that the time to remove half of the total discharge (t_{50}), which exhibits an exponential decay pattern, decreases with a rise in the voltage gradient. The maximum decrement of approximately 94% is observed for the applied voltage gradient of 0.15 V/mm compared to the ESC case. The pore water discharge is almost nil for all the applied voltage gradients except 0.025 V/mm for the subsequent loading stage from 9 to 100 kPa. This is mainly because the water present in the voids (called free water, which is present outside the diffuse double layer) can be removed by applying the overburden pressure. However, the electrokinetics help remove a significant portion of interstitial water (i.e., affected by capillary forces) and vicinal water (i.e., loosely bound to soil particles by adsorption) along with free water. The only water remaining after this stage is bound water, which can only be removed through thermal drying. Therefore, the expulsion of water finished after the first loading.

Similarly, removing 95% of the overall discharge takes much less time as the voltage gradient increases. The maximum reduction of 87% was observed after applying a voltage gradient of 0.15 V/mm; however, the reduction is minimal (~6%) for the applied voltage gradient of 0.025 V/mm compared to the ESC case. The overall discharge of pore water increases with the applied voltage gradient.

$$q_{t,E} = \frac{(q_0 + q_{96})}{1 + \exp\left(\frac{t - t_{50}}{dt}\right)} + q_{96} \quad (1)$$

where q_t, E = discharge at time t (hours) and applied voltage gradient (E), V/mm, measured in ml; q0= initial discharge at the start of the test = 0 ml; q_{96} = total discharge after the test, i.e., 96 hours in the current situation and this measured in ml; t_{50} = time for 50% of the total discharge and is measured in hours; dt = time constant, i.e., the slope at t_{50}. The above equation's parameters (q_0, q_{96}, t_{50}, and dt) depend on the voltage gradient and are represented below.

$$t_{50} = 113.23 * \exp\left(-{}^{E}/_{0.164}\right) + 3.21 \quad (2)$$

$$q_{96} = 600.44 + 5594.57 * E \quad (3)$$

$$dt = 93.91 * \exp\left({}^{-E}/_{0.14}\right) + 1.15 \quad (4)$$

here E = applied voltage gradient (V/mm). To develop a correlation for parameters (Eqs. (2)-(4)), the value of each parameter was evaluated from the plot of discharge vs time. After evaluating each parameter, a plot of this parameter (say, for instance, q_{96}) w.r.t. applied voltage gradient (E) was done. Finally, curve fitting was done to get the correlation equation for that parameter (say, for instance, q_{96}) with applied voltage gradient as an independent variable.

The generated pore water removal from soft clay improved after the inclusion of *e*-ESC, which is a complex process. The first and foremost important factor is the electro-osmotic flow under the influence of an electric field. The other factors responsible for this behavior are consolidation under the influence of applied surcharge and electrokinetics, electrochemical reactions in the clay, and enhancement in the permeability of the soft clay after the inclusion of *e*-ESC.

Subsequently, after applying the voltage gradient the discharge of pore water further increases, which in turn increases the settlement. The settlement was monitored at the top of the loading plate at a normalized radial distance of 0.60 from the center of the column (refer to Fig. 2). The introduction of a voltage gradient notably enhanced the consolidation rate of soft clay reinforced with *e*-ESC, with the most significant acceleration occurring during the early loading phase i.e., approximately 48, 37, 35, and 20%, was observed for the applied voltage gradient of 0.15, 0.10, 0.05, and 0.025 V/mm, respectively, after the application of the 9 kPa surcharge as compared to only 21% in the case of ESC improved clayey bed. Also, the increase in settlement with time (for an initial 6 hours) for the *e*-ESC case is mainly observed for 9 kPa loading. However, in subsequent loading stages, the settlements are immediate (within half an hour) with the applied load and vary marginally (i.e., less than 4%) with time, irrespective of voltage gradient. Most of the final settlement, i.e., approximately 67, 65, 63, and 43%, occurs before applying the 55 kPa load for the applied voltage gradient of 0.15, 0.10, 0.05, and 0.025 V/mm, respectively, approximately 38% for the ESC case. Additionally, the ultimate settlement rises as the voltage gradient increases, attaining a maximum of about 14% for the supplied voltage gradient of 0.15 V/mm compared to the ESC scenario. The settlement observations confirm that coupling ESC with electrokinetics (i.e., *e*-ESC) greatly accelerates consolidation settlement. This is mainly because electrokinetics helps remove free, interstitial and vicinal water and subsequent load application that helps reorient the pore structure and fabric of the soil (Pandey and Rajesh 2019) in the subsequent loading stage. Further, a higher applied voltage gradient leads to an increased amount of interstitial and vicinal water, resulting in higher settlement. This may also act as an additional surcharge and increase the magnitude of consolidation.

3.2 Distribution of moisture content and undrained shear strength

The moisture content of the clay bed can be reduced by extracting the pore water from it. One issue with electrokinetic treatment is the non-uniform spatial distribution of the moisture content due to electro-osmotic flow from anode to cathode. Therefore, to understand the spatial variation, the moisture content of the clay bed was determined at predefined locations before and after the treatment. Fig. 5(a) demonstrates the impact of a voltage gradient on the reduction of moisture content (RMC) between the electrodes measured at both depths of the clay bed. The RMC after treatment is defined as the ratio of the difference in initial water content (before treatment) and final water content (after treatment) to that of the initial water content. For the same applied voltage gradient, the difference in the average RMC at the mid-depth of the *e*-ESC improved clay bed was higher than at the surface. The margin of difference lessens as the applied voltage gradient rises. The average RMC measured at the surface for the applied voltage gradient of 0.025, 0.05, 0.10, and 0.15 V/mm was 1.18, 1.45, 1.73, and 1.86 times greater than the ESC case. The observed value at the mid-depth was 1.43, 1.71, 1.91, and 2.10 times that of the ESC for the applied voltage gradient of 0.025, 0.05, 0.10, and 0.15 V/mm, respectively. Further, the enhancement was uniform irrespective of location and voltage gradient. The combined effects of the hydraulic head gradient and voltage gradient may cause pore water flow from the anode to the cathode.

Fig. 5(b) shows the influence of voltage gradient on shear strength enhancement ($S_{u,E}$) measured both at the surface (Fig. 5(i)) and the mid-depth (Fig. 5(ii)) of soft clay after the test. In contrast to the ESC-strengthened case, the average $S_{u,E}$ value evaluated at the surface of the *e*-ESC case for applied voltage gradients of 0.025, 0.05, 0.10, and 0.15 V/mm was 1.12, 1.31, 1.46, and 1.71 times higher, respectively, while at the mid-depth it was 1.23, 1.43, 1.58, and 1.80 times higher, respectively. Regardless of the magnitude of the voltage gradient, the more significant improvement was recorded closer to the anode than the cathode. The lower strength increment near the cathode is due to the accumulation of migrated water in its vicinity. This accumulation of water may be reduced by altering the operational parameters, such as current intermittence and polarity reversal. The rise in $S_{u,E}$ of *e*-ESC improved clay bed is probably owing to the decrement in moisture content, enhanced soil bonding, and electrochemical interactions resulting from the electrokinetic process. The clear pattern of strength increment may not be fully explained by a reduction in the water content. There are various other factors that influence the extent of strength enhancement, including the type of electrodes used, soil characteristics, electrode spacing, applied voltage gradient, and the pattern of current application. Consequently, additional research is needed to determine the optimal combination of these parameters

3.3 Variation of current and power consumption

Fig. 6(a) illustrates the variation of electric current for different applied voltage gradients for *e*-ESC-reinforced soft clay. The variation of current is explained in three phases. The electric current increases in Phase I and reaches its maximum value. The peak gets sharper for steeper voltage gradients, i.e.,

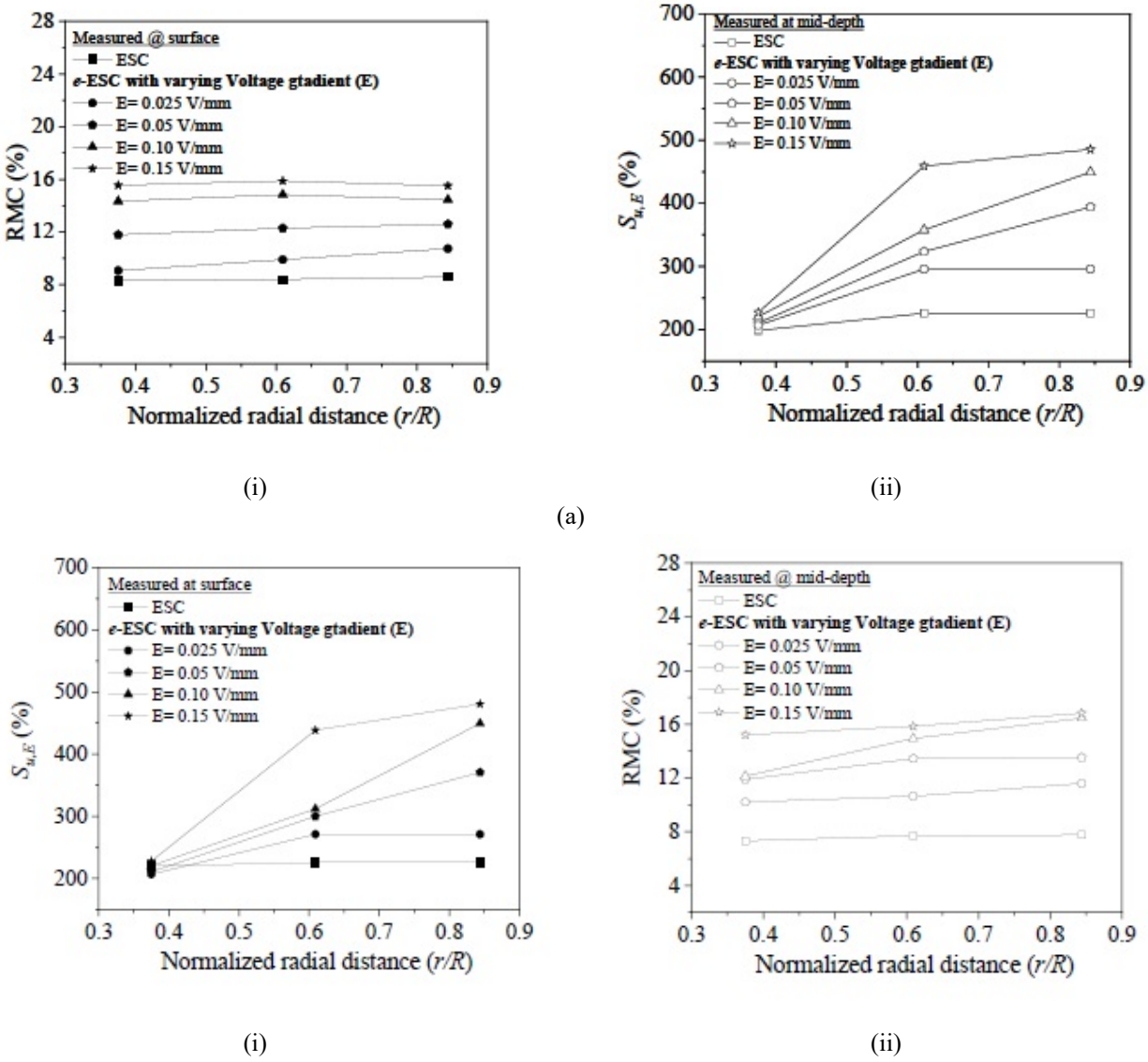

Fig. 5 Variation of (a) moisture content and (b) undrained shear strength of soft clay with normalized radial distance (r/R) at the (i) surface and (ii) mid-depth of clay bed

for 0.10 and 0.15 V/mm. The increase is moderate, and a more substantial peak was not seen for the 0.025 V/mm applied voltage gradient. A sharp decline in the electrical current from the peak was observed in phase II. During this phase, a maximum Fig. 6(a) illustrates the variation of electric current for different applied voltage gradients for *e*-ESC-reinforced soft clay. The variation of current is explained in three phases. The electric current increases in Phase I and reaches its maximum value. The peak gets sharper for steeper voltage gradients, i.e., for 0.10 and 0.15 V/mm. The increase is moderate, and a more substantial peak was not seen for the 0.025 V/mm applied voltage gradient. A sharp decline in the electrical current from the peak was observed in phase II. During this phase, a maximum decrement is seen at a voltage gradient of 0.15 V/mm, with the decrement rate ranging from 1.5 to 2% per hour. The decrement is gradual for the applied voltage gradient of 0.025 V/mm. The variation in the electric current depicts the alteration in the soil resistivity, as explained earlier. The average electric current consumed after the test (i.e., 96 hours) for the applied voltage gradient of 0.025, 0.05, 0.10, and 0.15 V/mm was 0.28, 0.50, 1.06, and 1.31 amperes, respectively. The variation in electric current is mainly due to changes in soil resistivity, other factors like conducting salts, temperature, and a reduction in void ratio. The increased temperature of the soft clay due to the applied voltage gradient leads to ohmic heating (not monitored in the present study), causing deterioration (discussed in the forthcoming section) and a reduction in the cross-sectional area of the anode, leading to the current drop. The basis for this performance may also be credited to the electrochemical passivation of electrodes, i.e., anode and cathode passivation (Sato and Okamoto 1981). This electrode passivation seriously disturbs the ionic transfer between the anode and the cathode and, in turn, interrupts their effectiveness. Nonetheless, the electrochemical

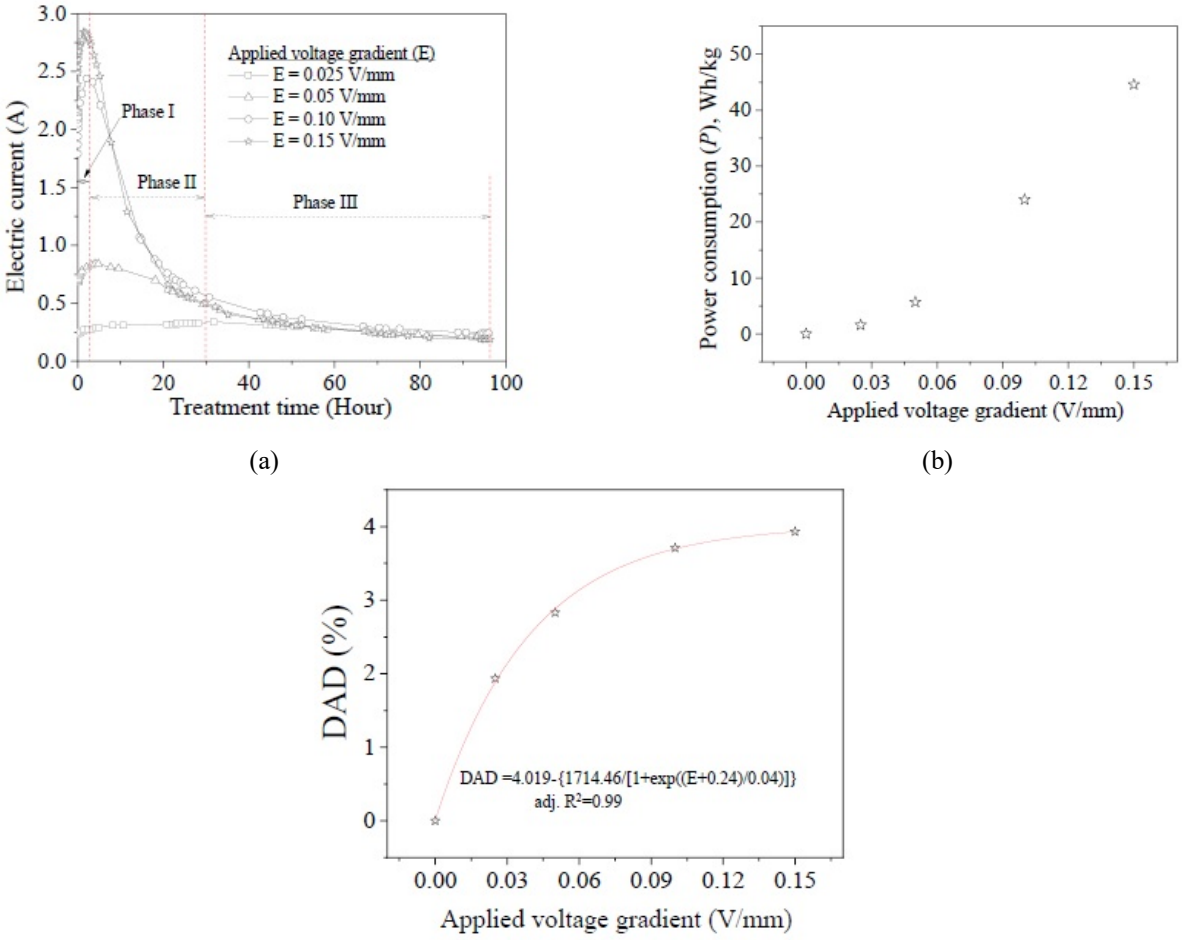

Fig. 6 Influence of applied voltage gradient on (a) variation of electric current (b) power consumption, and (c) anode deterioration

passivation could be minimized by using alternating current as a power source, which will be studied in the future.

Fig. 6(b) illustrates the impact of a voltage gradient on power consumption in treating clay. The power consumption (PC) per quantity of treated soil (Wh/kg) was assessed to determine the relative influence of the applied voltage gradient on the power usage through measurement following Eqs. (5) (Ortiz-Soto *et al.* 2018).

$$P = \int_0^t VIdt \Big/ W_S \tag{5}$$

Here, P = Power consumption in watt-hour per kg (Wh/kg), V = 80*E applied voltage among the electrodes (V), E voltage gradient (V/mm), I = Average electric current (A). t = total treatment time (hours), W_S = total weight of treated soft clay (kg), and the numerical value "80" represents the distance between the anode and the cathode in mm. The power consumption increases with the applied voltage gradient. The power consumption for applied voltage gradients of 0.05, 0.10, and 0.15 V/mm was 3.61, 15.21, and 28.21 times higher than that of the applied voltage gradient of 0.025 V/mm. Furthermore, compared to 0.10 V/mm, the applied voltage gradient of 0.15 V/mm consumed 1.86 times more electricity.

3.4 Electrochemical reaction and anode deterioration

During the electrokinetic treatment, the anode material decomposes with time. This decomposition is a result of electrolysis. The electrolysis and decomposition reactions occurring are presented in Eqs. (6)-(9). The electrochemical reactions occurring at the anode include the evolution of the oxygen (i.e., an oxidation reaction), as depicted in Equation 6. The evolution creates an acidic environment in the anode vicinity (explained in the forthcoming section). The second possible reaction involves anode corrosion, as illustrated in Eq. (7) (Pandey and Rajesh 2019), resulting in anode deterioration. According to Eqs. (8) and (9), the creation of hydrogen and hydroxide ions due to water reduction at the cathode promotes the establishment of a basic front. Under the influence of a voltage gradient, the acid and basic fronts created by electrochemical reactions will move in the opposite direction, meeting at a junction where the soil will become neutral. The basic front moves faster than the acid is transported (Asavadorndeja and Glawe 2005). Therefore, save from a few tiny portions near the anode, the acid front dominates the physicochemical reaction throughout the specimen (Acar *et al.* 1990).

$$2H_2O \rightarrow O_2 \uparrow +4H^+ + 4e^- \quad (6)$$

$$M \rightarrow M^{n+} + ne^- \quad (7)$$

$$2H_2O + 4e^- \rightarrow 2H_2 \uparrow +4OH^- \quad (8)$$

$$2H_3O^+ + 2e^- \rightarrow 2H_2O + H_2 \uparrow \quad (9)$$

The anode deterioration with applied voltage gradient is shown in Fig. 6(c) and presented in terms of the degree of anode deterioration (DAD). The DAD is evaluated as the ratio of loss of anode weight after the test to the weight at the start expressed in percentage. The fitted Eq. (10) expresses the non-linear variations of DAD with voltage gradient. The DAD expands as the applied voltage rises. A voltage gradient of 0.15 V/mm produced the maximum DAD. The increment compared to the applied voltage gradient of 0.025 was 1.46, 1.92, and 2.03 for the applied voltage gradient of 0.05, 0.10, and 0.15 V/mm, respectively. Further, the DAD was merely 5.6% higher for 0.15 V/mm than 0.10 V/mm, although power consumption was approximately twice for the same condition (refer to Fig. 6(b)).

$$DAD = 4.019 - \{{}^{1714.46}\Big/_{[1+exp\left[\frac{E+0.24}{0.04}\right]}\} \quad (10)$$

3.5 Visual observation

Fig. 7 shows the surface pattern observed after the test for the *e*-ESC-improved clayey soil. A distinct star-like pattern was observed for all the voltage gradients after the test (Figs. 7(a)-7(d)). This pattern could be seen at the soft clay's top and persisted to the bottom. The movement of water and eroded material from the anode to the cathode may be attributed to the evolution of these patterns. In addition, the eroded material forms a distinct color after electrochemical reactions, and the thickness of the pattern increases with the applied voltage gradient. Considering the electrode position, the region near the anode and the cathode were named the anode and cathode regions, respectively. The central region is

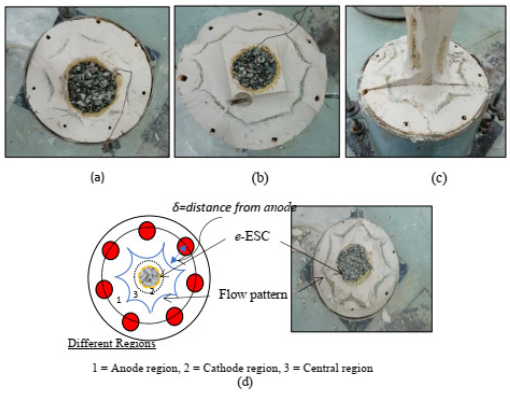

Fig. 7 Actual picture of the pattern formed for (a) 0.025 V/mm, (b) 0.05 V/mm, (c) 0.10 V/mm, and (c) 0.15 V/mm at the end of the test

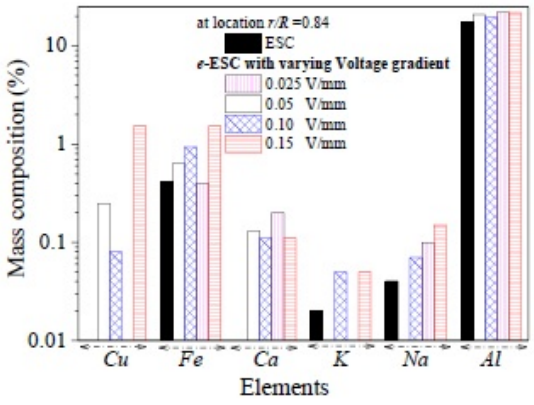

(a)

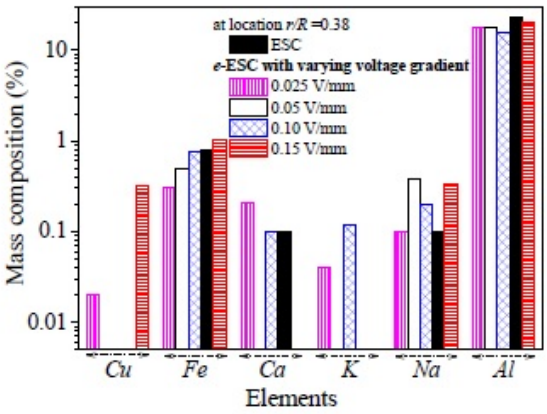

(b)

Fig. 8 Distribution of elements in the soil collected near (a) anode and (b) cathode at the end of the test

between them (Fig. 7(d)). The average radial distance of the flow pattern (δ) (refer to Fig. 7(d)) measured from the anode varied between 3 to 6.5 cm. The highest and lowest value is observed for the applied voltage gradient of 0.15 and 0.025 V/mm, respectively. This indicates the effectiveness of the higher voltage gradient in migrating the corroded anode material.

3.6 Modification in physiochemical properties

3.6.1 Element variation

Fig. 8 shows the impact of a voltage gradient on the constituent distribution in clay samples collected from the mid-depth, near the anode and cathode. The elements' mass composition modification is observed for the *e*-ESC case, irrespective of sampling location and voltage gradient. Anode corrosion and electrochemical processes, which are greatly influenced by the applied voltage gradient, cause the modification. The mass composition of Fe increases near the anode irrespective of the applied voltage gradient, which is equated to an ESC-improved clayey bed. The increment is maximum for the applied voltage gradient of 0.15 V/mm (i.e., 3.8 times), followed by 2.35, 1.6, and 1.03 times for the applied voltage gradient of 0.10, 0.05, and 0.025 V/mm, respectively. For an applied voltage gradient of 0.15 V/mm, the

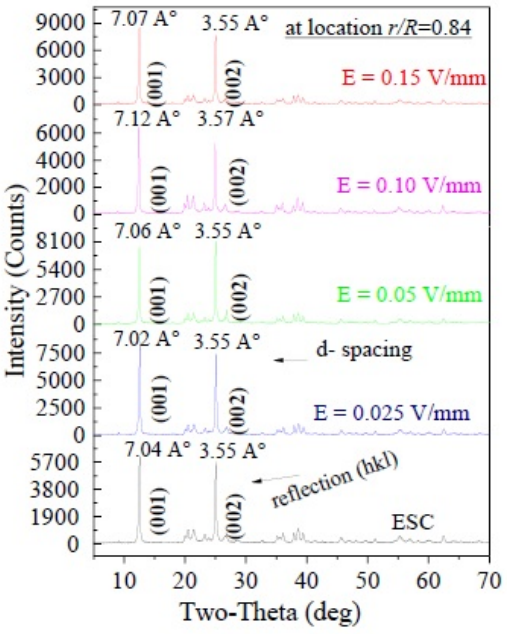

(a)

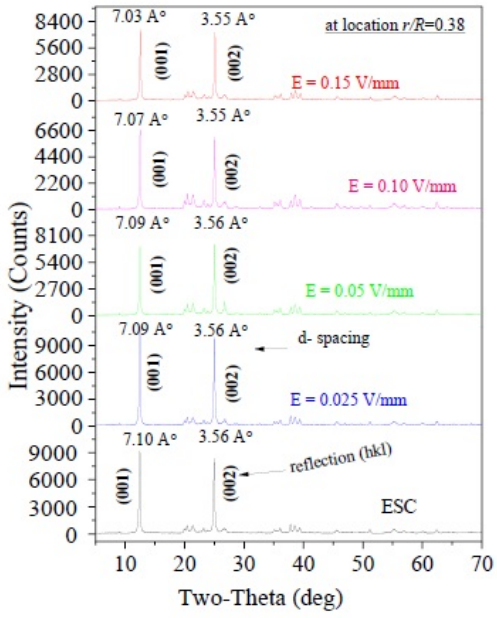

(b)

Fig. 9 X-ray diffractogram of soil collected near (a) anode and (b) cathode at the end of the test

Fe contents near the cathode rise by 1.28 times, whereas they fall for other cases than ESC-improved clay. As explained earlier, the alteration in the elemental content results from complex electrochemical reactions occurring in the clay and the electrode corrosion. The change is more pronounced close to the anode, indicating that the anode material was transported through the clayey soil. It is a crucial governing factor for hydraulic conductivity structural, mechanical, and other soil qualities. This alteration in the elemental composition reveals the effectiveness of *e*-ESC-improved clayey soil in altering the properties of the clay, which may be helpful in the case of expansive soils.

3.6.2 Alterations in clay mineralogy

The effect of a voltage gradient on the XRD pattern of the *e*-ESC-enhanced clayey bed is depicted in Fig. 9. The samples' X-ray diffraction (XRD) pattern (i.e., both before and after treatment) was obtained using two circle diffractometers (Rigaku MiniFlex 600). Additionally, to get the pattern, the CU-Kα (λ = 1.54059 A◦) radiation is applied at input voltage and current of 30 kV and 10 mA, respectively. The measurement range (i.e., 2-theta) adopted in the study varies between 5 to 70 degrees with a step width of 0.02˚/0.6(s) at 25 ℃ . Subsequently, patterns were processed using the commercial software MDI Jade. The analysis of the XRD pattern after the test for the clayey soil improved with ESC confirms the presence of two mineral phases irrespective of the locations (refer to Table 5). The number of mineral phases changed for *e*-ESC-improved clay.

As shown in Table 5, three mineral phases (i.e., kaolinite, dickite, and amesite) formed in the applied voltage gradient of 0.025, 0.05 and 0.15 V/mm irrespective of locations. The mineral phases formed for the applied voltage gradient of 0.10 V/mm were the same as in the ESC case. Still, the weight percentage of the minerals was different, as seen in Table 5, which presents the evolution of mineral phases at the end of the test. Further, the remarkable features of these phases are alterations in the location, intensity, and width of the peak. The modification of mineral phases in kaolin clay post-electrokinetic treatment with iron as the anode material may be influenced by factors like redox reactions, pH shifts, electroosmotic flow, and electrochemical alterations. During electrokinetic treatment, the movement of ions and redox reactions with the iron anode generate Fe^{2+} and Fe^{3+} ions, influencing mineral composition (as reported in the previous section). Electrokinetic-induced pH changes (reported in the forthcoming section) and electro-osmotic flow further impact the stability and distribution of mineral phases. Additionally, the electrochemical environment near the iron anode can lead to mineral dissolution and precipitation, causing transformations in specific mineral phases within the kaolin clay. Modifying mineral phases in clay through electrokinetic processes enhances strength, reduces permeability, and improves geotechnical properties. This tailored approach may benefit construction, remediation, and environmental applications.

The XRD peaks also explain the structural evolution that follows the test. Fig. 9 illustrates the modification in the d-spacing of the (001 and 002) reflection for the *e*-ESC-enhanced clay. The d-spacing of the (001) reflection near the anode (refer to Fig. 9(a)) does not show any precise trend, but it remains the same for the (002) reflection for the mentioned applied voltage gradients. However, at the location (*r/R*), 0.38 (refer to Fig. 9(b)), it reduces or remains the same for both (001 and 002) reflections. Earlier in the preceding section, the cause of this behavior was discussed.

3.6.3 pH alterations

In contrast to the initial pH, the pH value rises near the cathode while lowering near the anode, as seen in Fig. 10(a).

Table 5 Influence of voltage gradient on the evolution of the mineral phases at the end of the test

Location of sample	Reinforced Soft Clay	Applied Voltage Gradient (V/mm)	Mineral phases
Both ends	ESC	0	~ 87% Kaolinite, $Al_4(OH)_8(Si_4O_{10})$ and 13 % Dickite, $Al_2Si_2O_5(OH)_4$
Near Anode (r/R=0.84)	*e*-ESC	0.025	~ 76.2% Kaolinite, $Al_4(OH)_8(Si_4O_{10})$, 8.7% Amesite-2A, $(MgAl)_3(SiAl)_2O_5(OH)_4$ and 7.6 % Dickite, $Al_2Si_2O_5(OH)_4$, and a trace of others impurities
		0.05	~ 71.9% Kaolinite, $Al_4(OH)_8(Si_4O_{10})$, 19.3 % Dickite, $Al_2Si_2O_5(OH)_4$, and 6.1 Amesite-2A, $(MgAl)_3(SiAl)_2O_5(OH)_4$ and a trace of others impurities
		0.10	~ 85 % Kaolinite, $Al_4(OH)_8(Si_4O_{10})$ and 6.9 % Dickite, $Al_2Si_2O_5(OH)_4$, and a trace of others impurities
		0.15	~ 79.1% Kaolinite, $Al_4(OH)_8(Si_4O_{10})$, 7.6 % Dickite, $Al_2Si_2O_5(OH)_4$, and 6.5% Amesite-2A, $(MgAl)_3(SiAl)_2O_5(OH)_4$ and a trace of others impurities
Near cathode (r/R=0.38)	*e*-ESC	0.025	~ 67.6% Kaolinite, $Al_4(OH)_8(Si_4O_{10})$, 9.6 % Dickite, $Al_2Si_2O_5(OH)_4$, and 8.4% Amesite-2A, $(MgAl)_3(SiAl)_2O_5(OH)_4$ and a trace of others impurities
		0.05	~ 84.7% Kaolinite, $Al_4(OH)_8(Si_4O_{10})$, 19.3 % Dickite, $Al_2Si_2O_5(OH)_4$, and 3% Quartz, SiO_2
		0.10	~ 99 % Kaolinite, $Al_4(OH)_8(Si_4O_{10})$ and a trace of others
		0.15	~ 76.3% Kaolinite, $Al_4(OH)_8(Si_4O_{10})$, 10.1 % Dickite, $Al_2Si_2O_5(OH)_4$, and 7.4% Amesite-2A, $(MgAl)_3(SiAl)_2O_5(OH)_4$ and a trace of others impurities

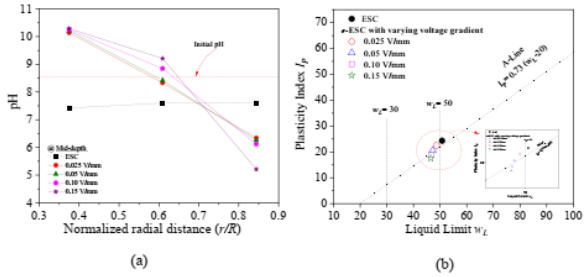

Fig. 10 Influence of applied voltage gradient on modification (a) pH and (b) Atterberg limit

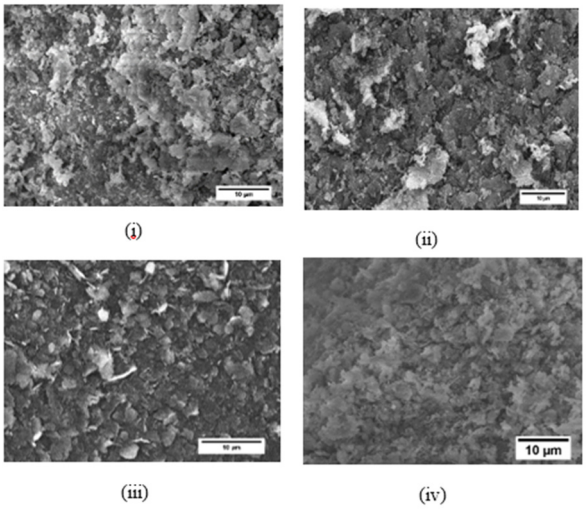

Fig. 11 Microfabric of the soft clay reinforced with *e*-ESC considering mild steel anode at an applied voltage gradient of (i) 0.025 V/mm, (ii) 0.05 V/mm, (iii) 0.10 V/mm and (iv) 0.15 V/mm at the end of the test (x 2000)

The pH rise is almost constant near the cathode (soil becomes alkaline), irrespective of the voltage gradient. However, the pH drops about the applied voltage gradient close to the anode (soil becomes acidic). A maximum decrement of approximately 47% was observed for the applied voltage gradient of 0.15 V/mm. Subsequently, the decrements for the applied voltage gradients of 0.10, 0.05, and 0.025 V/mm were 34, 18, and 15.605, respectively. The reason for this behaviour is explained earlier in detail. The alteration in the pH during electrokinetic treatment may enhance the contaminant mobility, induce chemical reactions, and stabilize pollutants. Further, it may also optimize soil remediation by influencing mineral solubility, electroosmotic flow, and microbial activity.

3.6.4 Atterberg's limits

Fig. 10(b) displays the impact of applied voltage on Atterberg's limits of *e*-ESC-improved clay on the plasticity chart. The Atterberg's limit was performed on the soil collected from the mid-depth of the clay bed. The reduction in the liquid limit is maximum for a voltage gradient of 0.15 V/mm (i.e., 8.37%), followed by 0.10 (i.e., 8%), 0.05 (i.e., 7%), and 0.025 (i.e., 4.20%) V/mm, respectively. Similarly, the maximum reduction in plasticity index was observed for the applied voltage gradient of 0.15 V/mm (i.e., 28%), followed by 0.10 (i.e., 23%), 0.05 (i.e., 15.58%), and 0.025 V/mm (i.e., 7.50%). This reduction in the Atterberg's limit changes the inorganic clay of high plasticity (CH) to silty clay of low compressibility (CL) for the applied voltage gradient of 0.025 and 0.05 V/mm; however, for 0.10 and 0.15 V/mm, it changes to inorganic silt of low compressibility (ML).

3.7 Structural evolution

According to Fig. 11, regardless of the applied voltage gradient, the clay particles tend to be dispersed and

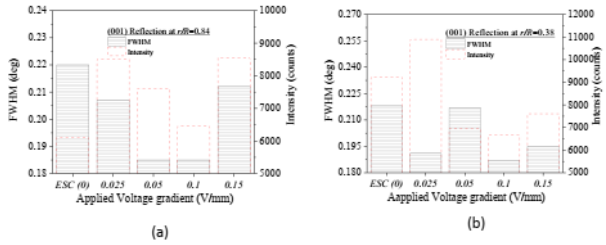

Fig. 12 Influence of voltage gradient on the evolution of FWHM and Intensity of (001) reflection near (a) anode and (b) cathode at the end of the test

deflocculated for *e*-ESC-improved clay beds. It exhibits a more dispersed fabric orientation for applied voltage gradients of 0.15 V/mm, followed by 0.10, 0.05, and 0.025 V/mm. Further, the intensity and full- -width at half maximum (FWHM) of the (001) reflection (refer to Fig. 9) for different applied voltage gradients is presented in Fig. 12. Near the anode, an increase inthe intensity of (001) reflection was observed for the *e*-ESC improved clay equated to the ESC reinforced case. The maximum increment was observed for the applied voltage gradient of 0.15 V/mm.

The FWHM obtained for the (001) reflection planes shows a decrement in value, regardless of the applied voltage gradient and sampling location. The maximum decrement of 16% was observed for 0.05 and 0.10 V/mm applied voltage gradient. The decrements were 6 and 3.6% for a voltage gradient of 0.025 and 0.15 V/mm near the anode (Fig. 12(a)). Further, the maximum decrement of 14% was observed near the cathode (Fig. 12(b)) for the applied voltage gradient of 0.10 V/mm, followed by 12.38, 10.55, and 0.46% for the applied voltage gradients of 0.025, 0.15, and 0.05 V/mm, respectively. This suggests that applying a voltage gradient changes the soft clay's structure and affects the intensity and FWHM of basal peaks. This alteration in d-spacing gives an idea of diffuse double-layer thickness, which is inversely proportional to d-spacing (Li *et al.* 2015). Soft clay's DDL thickness likely increased nearer the cathode but reduced near the anode. Reduced DDL thickness increases pore water flow and soft soil hydraulic characteristics.

4. Conclusions

In this study, the response of soft clay improved with an electrokinetic-assisted encased stone column is investigated, and the experimental results support these main conclusions:

• The highest total pore water discharge was recorded at an applied voltage gradient of 0.15 V/mm is approximately 2.01 times greater than that of the ESC control. Additionally, the time required to achieve 95% of total discharge was significantly reduced at higher voltage gradients. At 0.15 V/mm, the reduction was approximately 87%, while at 0.025 V/mm, the reduction was only around 6%.

• Settlement behavior was also affected by the voltage gradient. The greatest overall settlement (~14%) occurred at 0.15 V/mm, followed by ~3% at 0.10 V/mm and ~0.5% at 0.05 V/mm, compared to ESC alone. The application of e-ESC notably accelerated the rate of consolidation, with 63–67% of total settlement under higher gradients (E ≥ 0.5 V/cm) occurring before the third stage of incremental loading.

• Under identical surcharge loading conditions, *e*-ESC treatment consistently reduced the moisture content of the clay bed. This moisture reduction became more pronounced as the voltage gradient increased.

• The average undrained shear strength ($S_{u,\ E}$) at the soil surface was higher for *e*-ESC-treated samples across all tested depths and voltage levels, compared to the reference. However, strength improvement was spatially uneven, with greater improvement near the anode and diminishing toward the cathode.

• Electric current behavior varied markedly during the initial 30 hours of high-voltage tests. At steeper voltage gradients, current peaks were sharper and more pronounced, whereas lower gradients produced more gradual increases without distinct peaks.

• Power consumption rose with increasing voltage gradients. Relative to the baseline of 0.025 V/mm, the energy used per kilogram of treated soil increased by factors of approximately 3.61, 15.21, and 28.21 for 0.05, 0.10, and 0.15 V/mm, respectively.

• The electrokinetic-assisted encased stone column can alter the chemical composition, pH, Atterberg limits, mineral phases, and microfabric of clayey soil. Therefore, the proposed technique can be utilized to accelerate the rate of consolidation, arrest long-term settlement, soil remediation, strengthen stability issues of embankment, control the swell-shrink behaviour, etc.

Acknowledgments

The Science and Engineering Research Board, Department of Science and Technology, India (Grant Nos. SERB/F/4638/2013-14 and No. CRG/2018/004612), as well as the Initial Grant from IIT Kanpur (Grant No. 20110145), are both gratefully acknowledged by the authors.

References

Acar, Y.B., Gale, R.J. and Putnam, G. (1990), "Electrochemical processing of soils: Theory of pH gradient development by diffusion and linear convection", *J. Environ. Sci. Health.*, **25**, 687-714. https://doi.org/10.1080/10934529009375590.

Al-Khafaji, K.R., Fattah, M.Y. and Al-Recaby, M.K. (2024), "Assessment of creep improvement of organic soil improved by stone columns", *Geomech. Eng.*, **38**(2), 191-203. https://doi.org/10.12989/gae.2024.38.2.191.

Asavadorndeja, P. and Glawe, U. (2005), "Electrokinetic strengthening of soft clay using the anode depolarization method", *Bull. Eng. Geol. Environ.*, **64**, 237-245. https://doi.org/10.1007/s10064-005-0276-7.

Bergado, D.T., Sasanakul, I. and Horpibulsuk, S. (2003), "Electro-osmotic consolidation of soft Bangkok clay using copper and carbon electrodes with PVD", *Geotech. Test. J.*, **26**(3), 277-288. https://doi.org/10.1520/GTJ11309J.

Chien, S.C., Ou, C.Y. and Wang, M. (2009), "Injection of saline solutions to improve the electro-osmotic pressure and consolidation of foundation soil", *Appl. Clay Sci.*, **44**, 218-224. https://doi.org/10.1016/j.clay.2009.02.006.

Chummar, A.V. (1972), "Bearing capacity theory from

experimental results", *J. Soil Mech. Found. Div*., **98**(12), 1311-1324. https://doi.org/10.1061/JSFEAQ.0001816.

Demir, A. and Sarici, T. (2017), "Bearing capacity of footing supported by geogrid encased stone columns on soft soil," *Geomech. Eng*., **12**(3), 417-439. https://doi.org/10.12989/gae.2017.12.3.417.

Dinarvand, R. and Ardakani, A. (2022), "Shear behavior of geotextile-encased gravel columns in silty sand-Experimental and SVM modeling", *Geomech. Eng*., **28**(5), 505-520. https://doi.org/10.12989/gae.2022.28.5.505.

Dutta, S. and Mandal, J.N. (2017), "Model studies on encased fly ash column – geocell composite systems in soft clay", *J. Hazard. Toxic Radioact*., **21**, 1-15. https://doi.org/10.1061/(ASCE)HZ.2153-5515.0000353.

Hamza, O. and Ikin, J. (2020), "Electrokinetic treatment of expansive desiccated clay", *Geotechnique*, **70**(5), 214-235. https://doi.org/10.1680/jgeot.18.P.266.

Hausmann M.R. (1991), *Engineering Principles of Ground Modification*. McGraw-Hill, New York, USA.

Jaiswal, A. and Kumar, R. (2023), "Influence of dual layer confinement on lateral load capacity of stone columns: An experimental investigation", *Geomech. Eng*., **32**(6), 567-581. https://doi.org/10.12989/gae.2023.32.6.567.

Jones, C.J.F.P., Lamont-Black, J. and Glendinning, S. (2011), "Electrokinetic geosynthetics in hydraulic applications", *Geotext. Geomembranes*, **29**, 381-390. https://doi.org/10.1016/j.geotexmem.2010.11.011.

Malarvizhi, S.N. and Ilamparuthi, K. (2007), "Comparative study on the behavior of encased stone column and conventional stone column", *Soils Found.*, **47**(5), 873-885. https://doi.org/10.3208/sandf.47.873.

Mazumder, T., Rolaniya, A.K. and Ayothiraman, R. (2018), "Experimental study on behaviour of encased stone column with tyre chips as aggregates", *Geosynth. Int.,* **25**(3), 259-270. https://doi.org/10.1680/jgein.18.00006.

Methacanon, P., Weerawatsophon, U., Sumransin, N., Prahsaran, C. and Bergado, D.T. (2010), "Properties and potential application of the selected natural fibers as limited life geotextiles", *Carbohyd. Polym*., **82**, 1090-1096. https://doi.org/10.1016/j.carbpol.2010.06.036 .

Mohamedelhassan, E. and Shang, J.Q. (2001), "Effects of electrode materials and current intermittence in electro-osmosis", *Proc. Inst. Civ. Eng.: Ground Improv*., **5**, 3-11. https://doi.org/10.1680/grim.2001.5.1.3

Murugesan, S. and Rajagopal, K. (2007), "Model tests on geosynthetic-encased stone columns", *Geosynth. Int.*, **14**(6), 346-354. https://doi.org/10.1680/gein.2007.14.6.346

Ortiz-Soto, R., Leal, D., Gutierrez, C., Aracena, A., Rojo, A., Hansen, H.K. (2019), "Electrokinetic remediation of manganese and zinc in copper mine tailings", *J. Hazard. Mater*., **365**, 905-911. https://doi.org/10.1016/j.jhazmat.2018.11.048.

Pandey, B.K. and Rajesh, S. (2019), "Enhanced engineering characteristics of soils by electro-osmotic treatment: An overview.", *Geotech. Geol. Eng*., **37**(6), 4649-4673. https://doi.org/10.1007/s10706-019-00973-3.

Pandey, B.K., Rajesh, S. and Chandra, S. (2021), "Performance enhancement of encased stone column with conductive natural geotextile under k0 stress condition", *Geotext. Geomembranes*, **49**(5), 1095-1106. https://doi.org/10.1016/j.geotexmem.2021.03.004.

Pandey, B.K., Rajesh, S. and Chandra, S. (2022a), "Performance of soft clay reinforced with encased stone column: A systematic review", *Int. J. Geosynth. Ground Eng.*, **8**, https://doi.org/10.1007/s40891-022-00387-x.

Pandey, B.K., Rajesh, S. and Chandra, S. (2022b), "Time-dependent behaviour of embankment on clayey soil improved using stone columns encased by geotextiles", *Transp. Geotech.*, **36**, 100809. https://doi.org/10.1016/j.trgeo.2022.100809.

Pedersen, K.B., Jensen, P.E., Ottosen, L.M. and Barlindhaug, J. (2018), "The relative influence of electrokinetic remediation design on the removal of As, Cu, Pb and Sb from shooting range soils", *Eng. Geol.*, **238**, 52-61. https://doi.org/10.1016/j.enggeo.2018.03.005.

Rajesh, S. (2017), "Time-dependent behaviour of fully and partially penetrated geosynthetic encased stone columns", *Geosynth. Int*., **24**(1), 60-71. https://doi.org/10.1680/jgein.16.00015.

Rezaei-Hosseinabadi, M.J., Bayat, M., Nadi, B. and Rahimi, A. (2022), "Sustainability utilization of steel slag as a granular column for ground improvement in geotechnical projects", *Case Stud. Constr. Mater.*, **17**, e01333. https://doi.org/10.1016/j.cscm.2022.e01333.

Sato, N. and Okamoto, G. (1981), "Electrochemical passivation of metals", (Eds., Bockris, J.O., Conway, B.E., Yeager, E., White, R.E.), *Electrochemical Materials Science. Comprehensive Treatise of Electrochemistry*, **4.** Springer, Boston, MA. https://doi.org/10.1007/978-1-4757-4825-3_4.

Sun, J., Lu, M., Xu, B. and Shan, J. (2024), "Consolidation of high replacement ratio stone column-reinforced ground: Analytical solutions incorporating clogging effect", *J. Rock Mech. Geotech. Eng*., https://doi.org/10.1016/j.jrmge.2023.12.011.

Tandel, Y.K., Solanki, C.H. and Desai, A.K. (2014), "Field behaviour geotextile reinforced sand column", *Geomech. Eng*., **6**(2), 195-211. https://doi.org/10.12989/gae.2014.6.2.195.

Wang, L., Huang, P., Liu, S. and Alonso, E. (2020), "Analytical solution for non-linear consolidation of combined electroosmosis-vacuum-surcharge preloading", *Comput. Geotech*., **121**, 103484. https://doi.org/10.1016/j.compgeo.2020.103484.

Yu, Y., Wang, Z. and Sun, H. (2020), "Optimal design of stone columns reinforced soft clay foundation considering design robustness", *Geomech. Eng*., **22**(4), 305-318. https://doi.org/10.12989/gae.2020.22.4.305.

Zhang, Y., Chan, D. and Wang, Y. (2012), "Consolidation of composite foundation improved by geosynthetic-encased stone columns", *Geotext. Geomembranes*, **32**, 10-17. https://doi.org/10.1016/j.geotexmem.2011.10.006.

Zhang, X., Yoo, C., Chen, J.F. and Gu, Z.A. (2022), "Numerical modelling of floating geosynthetic-encased stone column-supported embankments with basal reinforcement", *Geotext. Geomembranes*, **50**, 720-736. https://doi.org/10.1016/j.geotexmem.2022.03.012.

Zhou, J., Tao, Y.L., Xu, C.J., Gong, X.N. and Hu, P.C. (2015), "Electro-osmotic strengthening of silts based on selected electrode materials", *Soils Found*., **55** (5), 1171-1180. https://doi.org/10.1016/j.sandf.2015.09.017.

CC